Controls on the strength and structure of the Atlantic meridional overturning circulation in climate models

Manali S. Nayak[1,2,*], David B. Bonan[3,*], Emily R. Newsom[3], Andrew F. Thompson[3]

[1]Department of Physics, The Ohio State University, Columbus, OH, USA
[2]Department of Atmospheric Sciences, University of Washington, Seattle, WA, USA
[3]Environmental Science and Engineering, California Institute of Technology, Pasadena, CA, USA
[*]These authors contributed equally to this work.

Key Points:

- The thermal-wind expression captures the intermodel spread in mean-state AMOC strength across GCMs.
- Intermodel variations in the AMOC strength are related to intermodel variations in the overturning scale depth.
- GCMs with a larger scale depth exhibit larger surface buoyancy loss and weaker stratification in the North Atlantic, and a stronger AMOC.

Corresponding author: Manali Nayak; David Bonan, manalin@uw.edu; dbonan@caltech.edu

Abstract

State-of-the-art climate models simulate a large spread in the mean-state Atlantic meridional overturning circulation (AMOC), with strengths varying between 12 and 25 Sv. Here, we introduce a framework for understanding this spread by assessing the balance between the thermal-wind expression and surface water mass transformation in the North Atlantic. The intermodel spread in the mean-state AMOC strength is shown to be related to the overturning scale depth: climate models with a larger scale depth tend to also have a stronger AMOC. Intermodel variations in the overturning scale depth are also related to intermodel variations in North Atlantic surface buoyancy loss and stratification. We present a physically-motivated scaling relationship that links the scale-depth variations to buoyancy forcing and stratification in the North Atlantic, and thus connects North Atlantic surface processes to the interior ocean circulation. These results offer a framework for reducing mean-state AMOC biases in climate models.

Plain Language Summary

The Atlantic meridional overturning circulation – a branch of ocean currents confined to the Atlantic basin – strongly influences regional climate by redistributing heat, freshwater and carbon throughout the ocean. Understanding the processes that control the strength of this circulation feature, particularly in climate models, remains an active area of research. In this study, we introduce a conceptual framework to understand the dynamics that produce a large spread in the strength of the Atlantic meridional overturning circulation across climate models. We find that climate models that exhibit stronger circulation also have a deeper circulation. We introduce another expression to show that models with a deeper circulation also have stronger surface buoyancy loss and weaker stratification in the North Atlantic, which allows for more formation of dense waters that supply the southward flowing component of the Atlantic meridional overturning circulation. This conceptual framework provides a pathway to reduce climate model biases in simulating the present-day Atlantic meridional overturning circulation.

1 Introduction

The ocean's global overturning circulation (GOC) is a complex system of currents that connects different ocean basins (Gordon, 1986; Broecker, 1991; Lumpkin & Speer, 2007; Talley, 2013). The branch of the GOC that is localized to the Atlantic basin, often referred to as the Atlantic meridional overturning circulation (AMOC), is a unique feature of the GOC because it transports heat northward at all latitudes (Ganachaud & Wunsch, 2003) and ventilates the upper 2000 m of the ocean (Buckley & Marshall, 2016). The AMOC plays a central role in modulating regional and global climate by impacting Atlantic sea-surface temperatures, which cause changes to the African and Indian monsoon, the summer climate over North America and Western Europe, and Arctic sea ice (Zhang & Delworth, 2006; Mahajan et al., 2011; Zhang et al., 2019). The AMOC is also thought to play a leading order role in setting the peak of tropical rainfall in the Northern Hemisphere (Frierson et al., 2013; Marshall et al., 2014). For these reasons, understanding what controls the strength and structure of the AMOC remains a central goal of climate science.

Despite decades of research on the AMOC, the intermodel spread in the mean-state AMOC strength across state-of-the-art global climate models (GCMs) remains large (e.g., Schmittner et al., 2005; Cheng et al., 2013; Reintges et al., 2017; Weijer et al., 2020; Jackson & Petit, 2023). For example, in pre-industrial control (piControl) simulations from GCMs participating in Phase 6 of the Coupled Model Intercomparison Project (CMIP6), the mean-state AMOC strength, which is calculated as the maximum of the meridional overturning circulation in the Atlantic basin, varies between 12 and 25 Sv (1 Sv $\equiv 10^6$ m^3 s^{-1}; Figure 1). GCMs also simulate a large intermodel spread in the AMOC strength at all depths. GCMs with a weaker maximum AMOC (e.g., IPSL-CM6A-LR) tend to exhibit a weaker AMOC throughout the upper cell, whereas those with a stronger maximum AMOC (e.g., NorESM2-MM) tend to exhibit a stronger AMOC throughout the upper cell (Figure 1). There is also a close relationship between the strength and depth of the AMOC in GCMs: the depth of the maximum AMOC strength tends to be greater in GCMs with a stronger AMOC (compare circles in Fig. 1). The large intermodel spread in both the strength and structure of the mean-state AMOC leads to a key question: What causes the intermodel spread in the mean-state AMOC strength across GCMs?

Historically, variations in the AMOC strength have been attributed to processes affecting surface buoyancy fluxes in the North Atlantic, as this is where North Atlantic Deep Water (NADW) forms (e.g., Klinger & Marotzke, 1999; Marotzke & Klinger, 2000; Samelson, 2009; Wolfe & Cessi, 2011; Radko & Kamenkovich, 2011; Sévellec & Fedorov, 2016; Wang et al., 2010; Heuzé, 2021; Lin et al., 2023; Jackson & Petit, 2023). For example, Lin et al. (2023) found that GCMs with a stronger mean-state AMOC strength tend to have a less stratified North Atlantic, which permits deeper open-ocean convection and thus stronger NADW formation. Studies have also related the AMOC strength to the meridional density difference between the low- and high-latitude regions of the Atlantic basin (Stommel, 1961; Hughes & Weaver, 1994; Thorpe et al., 2001). However, subsequent work found that meridional density gradients do not control the AMOC strength (De Boer et al., 2010). Other work has argued that the Southern Ocean plays a primary role in setting the strength and structure of the AMOC through a combination of wind-driven Ekman transport and eddy transport (Toggweiler & Samuels, 1998; Gnanadesikan, 1999; Vallis, 2000; Wolfe & Cessi, 2010; De Boer et al., 2010; Sévellec & Fedorov, 2011; Wolfe & Cessi, 2011; Nikurashin & Vallis, 2012; Marshall et al., 2017; Saenko et al., 2018), and surface buoyancy forcing (Shakespeare & Hogg, 2012; Ferrari et al., 2014; Jansen & Nadeau, 2016; Baker et al., 2020). Yet, the equilibrium AMOC strength in coupled GCMs has been shown to be relatively unchanged with strengthened winds over the Southern Ocean (Jochum & Eden, 2015; Gent, 2016), potentially due to compensating effects from eddy transport (Abernathey et al., 2011). Collectively, these results do not point to a clear mechanism for the large intermodel spread in the mean-state AMOC strength across coupled GCMs.

Seminal work by Gnanadesikan (1999) showed that the strength of NADW formation (and thus the strength of the AMOC) can be related to the meridional pressure gradient of the Atlantic basin. De Boer et al. (2010) took a similar approach and showed that an expression based on thermal-wind balance accurately emulates the strength of the AMOC in ocean-only simulations. And more recently, Jansen et al. (2018) and Bonan et al. (2022) showed that variations in the AMOC strength across more sophisticated ocean-only and coupled GCMs could be described by a simple thermal-wind expression. These studies suggest that the thermal-wind expression, which links meridional density gradients to meridional volume transport under an assumption of mass conservation between zonal and meridional volume transport, provides a physically-motivated framework for understanding the intermodel spread in the mean-state AMOC strength. Yet, in coupled GCMs, it is unclear which aspect of the thermal-wind balance contributes to the intermodel spread in AMOC strength. Does the meridional density difference or overturning scale depth contribute more to the intermodel spread in AMOC strength? Furthermore, it is unclear how to relate the circulation implied by the thermal-wind expression to the circulation implied by surface water mass transformation, which must be equivalent in steady state. Our understanding of how surface and interior ocean processes contribute to the intermodel spread in mean-state AMOC strength remains unclear.

In this study, we introduce a framework for understanding the intermodel spread in the mean-state AMOC strength in coupled GCMs by linking the thermal-wind expression to surface water mass transformation in the North Atlantic. In what follows, we first describe the CMIP6 output and the thermal-wind expression. We then show that the thermal-wind expression accurately emulates the strength of the AMOC in coupled GCMs. We find that the intermodel spread in the mean-state AMOC strength is dominated by the intermodel spread in the overturning scale depth. We further find that the overturning scale depth can be related to North Atlantic surface buoyancy fluxes and stratification. GCMs with a deeper scale depth tend to have stronger North Atlantic surface buoyancy loss and weaker North Atlantic stratification. These results provide a pathway for reducing biases in the mean-state AMOC across GCMs.

2 Data and Methods

2.1 CMIP6 output

This study uses monthly output from 22 piControl r1i1p1f1 simulations for GCMs participating in CMIP6 (see Figure 1 for model names). The model output is averaged over the last 200 years of the piControl simulations.

The AMOC strength is identified from the meridional overturning streamfunction (msftmz and msftmy) and is defined as the maximum value of msftmz or msftmy in the Atlantic basin poleward of 30°N and below 500 m. The choice of 500 m avoids volume flux contributions associated with the subtropical ocean gyres. The surface buoyancy flux (discussed in detail below), is computed using the net surface heat flux (hfds) and net surface freshwater flux (wfo). Finally, ocean potential density referenced to 1000 dbar is calculated from ocean potential temperature (thetao) and ocean absolute salinity (so).

2.2 Surface buoyancy flux

The surface buoyancy flux F_b (units of $\mathrm{m^2\ s^{-3}}$) is calculated using a linear equation of state:

$$F_b = \underbrace{\frac{g\alpha}{\rho_0 c_p} Q_s}_{\text{thermal}} + \underbrace{g\beta S_0 F_s}_{\text{haline}}, \tag{1}$$

where g is the gravitational acceleration (9.81 $\mathrm{m\ s^{-2}}$), ρ_0 is a reference density of seawater (1027.5 $\mathrm{kg\ m^{-3}}$), c_p is the heat capacity of seawater (4000 $\mathrm{J\ kg^{-1}\ K^{-1}}$), α is the thermal

expansion coefficient (-1.5×10^{-4} K^{-1}), β is the haline contraction coefficient (7.6×10^{-4} kg g^{-1}), and S_0 is reference salinity (35 g kg^{-1}). Here, Q_s is the net surface heat flux (in W m^{-2}) and represents the thermal component, and F_s is the net surface freshwater flux (in m s^{-1}) and represents the haline component. Both are defined as positive downwards meaning positive for ocean heat gain and ocean freshwater gain. Note that this linear equation of state, which assumes constant values of α and β, does not diverge significantly from the general case where the coefficients are spatially variable.

3 Controls on the AMOC in CMIP6

We begin by applying the thermal-wind expression to each individual CMIP6 piControl simulation. Previous studies have shown that the thermal-wind expression, which links the strength of the overturning circulation to the density contrast between the northern sinking region and more southern latitudes, accurately approximates the AMOC strength in GCMs (De Boer et al., 2010; Jansen et al., 2018; Johnson et al., 2019; Sigmond et al., 2020; Bonan et al., 2022). The interior overturning circulation ψ_i diagnosed by the thermal-wind expression is given by

$$\psi_i = \frac{g}{2\rho_0 f_0} \Delta_y \rho H^2, \tag{2}$$

where f_0 is the Coriolis parameter (1×10^{-4} s^{-1}), $\Delta_y \rho$ is the meridional density difference between the North Atlantic and low-latitude Atlantic (kg m^{-3}), and H is the scale depth (m).

Following De Boer et al. (2010), $\Delta_y \rho$ is calculated as the difference in potential density (referenced to 1000 dbar) between the North Atlantic (area-averaged from 40°N to 60°N) and the low-latitude Atlantic (area-averaged from 30°S to 30°N) over the upper 1000 meters of the Atlantic basin. This accounts for density variations in the upper cell. H is calculated as the depth where the depth-integrated $\Delta_y \rho(z)$ (for the same regional domains) equals the vertical mean of the depth-integrated $\Delta_y \rho(z)$. In other words, H is calculated as

$$\int_{-H}^{0} \Delta_y \rho(z)\, dz = \frac{1}{D} \int_{-D}^{0} \Delta_y \rho(z) z\, dz, \tag{3}$$

where D is the depth of the entire water column. This estimate of H is approximately the depth of maximum zonal volume transport (De Boer et al., 2010).

The thermal-wind expression (Eq. 2) accurately emulates the AMOC strength in each GCM, accounting for approximately 84% of the intermodel variance and having a root-mean-square error of approximately 2 Sv (Fig. 2a). The strong agreement between the AMOC strength and thermal-wind expression in each GCM suggests that intermodel differences in the AMOC strength can be attributed to intermodel differences in $\Delta_y \rho$ and H (Fig. 2b).

3.1 Controls on the AMOC strength

Based on the success of the thermal-wind expression in emulating the AMOC strength in GCMs, we perform a perturbation analysis of $\Delta_y \rho$ and H to explore which term contributes most to the intermodel spread in the AMOC strength. Defining the multi-model mean as $\overline{(\cdot)}$ and deviations from the multi-model mean (the intermodel spread) as $(\cdot)'$, the intermodel spread can be approximated as

$$\psi_i' = \frac{g}{2\rho_0 f_0} \left(\underbrace{\Delta_y \rho' \overline{H}^2}_{(1)} + \underbrace{\overline{\Delta_y \rho} 2 \overline{H} H'}_{(2)} + \underbrace{\epsilon}_{(3)} \right), \tag{4}$$

where (1) represents intermodel variations in the AMOC strength due to intermodel variations in $\Delta_y \rho$; (2) represents intermodel variations in the AMOC strength due to intermodel variations in H; and (3) represents higher order residual terms.

The intermodel spread in the AMOC strength is more strongly dependent on the intermodel spread in H, with $\Delta_y \rho$ playing a secondary role (compare green and orange bars in Fig. 2c). The residual terms contribute little to the intermodel spread of the AMOC strength (see grey bars in Fig. 2c). Intermodel variations in H account for approximately 76% of the intermodel variance in AMOC strength (green bars, Fig. 2c), whereas intermodel variations in $\Delta_y \rho$ account for approximately 31% of the intermodel variance (orange bars, Fig. 2c). Note, however, that H and $\Delta_y \rho$ are somewhat correlated (De Boer et al., 2010) and therefore are not entirely independent of each other. Yet, variations in H have an outsized importance, most evident in GCMs with extremely weak or strong AMOC strengths. For example, GCMs which exhibit the weakest mean-state AMOC strength (IPSL-CM6A-LR, CanESM5, UKESM1-0-LL) tend to have the smallest H, while GCMs which exhibit the strongest mean-state AMOC strength (NorESM2-MM, NorESM2-LM, MPI-ESM1-2-LR) tend to have the largest H.

Physically, these results show that a stronger AMOC is linked to a stronger meridional density gradient. However, differences in the AMOC strength across GCMs are primarily driven by differences in the overturning scale depth (Fig. 2c), which is related to the spatial distribution of outcropping density classes in the North Atlantic, rather than the total difference in density between low and high latitude water masses.

3.2 Connection to North Atlantic processes

The strong control of H on the mean-state AMOC strength in GCMs suggests a fundamental relationship between H and surface processes in the North Atlantic. In steady-state, the interior overturning circulation ψ_i implied by the thermal-wind expression must balance the volume transport associated with the surface water mass transformation, assuming interior diabatic processes are relatively small. Building on earlier work by Speer and Tziperman (1992) and motivated by application of residual mean theory to the surface buoyancy budget in the Southern Ocean (Marshall & Radko, 2003), we expect the North Atlantic overturning transport in the surface mixed layer ψ_s to depend on the magnitude of the surface buoyancy flux F_b and the meridional surface buoyancy gradient $\partial b/\partial y$. However, because the region of surface water mass transformation in the North Atlantic varies widely across GCMs (e.g., Jackson & Petit, 2023), we modify this relationship to express ψ_s in terms of the vertical stratification N^2 of the North Atlantic

$$N^2 \equiv -\frac{g}{\rho_0}\frac{\partial \rho}{\partial z}, \tag{5}$$

and the isopycnal slope S of the North Atlantic

$$S \equiv -\frac{\partial b/\partial y}{\partial b/\partial z} \approx \frac{H}{L_y}, \tag{6}$$

where L_y is a meridional length scale (3000 km) that represents the meridional distance over which interior isopycnals tilt up towards their surface outcrop location. In other words, an estimate of the surface meridional density gradient can be derived from a bulk average of interior ocean processes (i.e., $\partial b/\partial y \approx N^2 S$) to alleviate concerns about the exact distribution of $\partial b/\partial y$ in each GCM. This results in the relationship

$$\psi_s = \frac{F_b}{N^2}\frac{L_x}{S}, \tag{7}$$

where F_b is the North Atlantic surface buoyancy flux and L_x is the zonal width of the Atlantic basin at the latitude of maximum flow (10000 km). This relationship assumes that the interior isopycnals that outcrop in the North Atlantic are geometrically confined due to land masses, such that L_y is constant.

Assuming steady-state conditions and that interior diabatic processes in the AMOC density classes are negligible, Eqs. (2) and (7) can be combined to relate H in terms of North

Atlantic properties,

$$H = \left(\frac{F_b}{N^2} \frac{L_x L_y}{\Delta_y \rho} \frac{2\rho_0 f_0}{g} \right)^{1/3}. \quad (8)$$

Eq. (8) shares a similar form to other scalings for H (Gnanadesikan, 1999; Klinger & Marotzke, 1999; Marotzke & Klinger, 2000; Youngs et al., 2020). For example, Klinger and Marotzke (1999) found a power of 1/3 dependence on H but instead related H to the vertical diffusivity of the interior ocean. Eq. (8) describes the sensitivity of H to North Atlantic processes, specifically the magnitude of the North Atlantic stratification and surface buoyancy flux, rather than interior ocean or Southern Ocean processes. A stronger F_b or weaker N^2 is associated with a deeper H.

The surface buoyancy flux F_b is area-averaged in the region of water mass transformation (40°N to 70°N in the Atlantic basin). The vertical stratification N^2 is estimated as the area-averaged value for the same regional domain and further averaged over the upper 1000 m (excluding 0-100 m, which represents the ocean's surface mixed layer). This captures variations in stratification associated with outcropping isopycnals.

Figure 3a shows a comparison of H (black bars) diagnosed from GCMs and H (black hatched bars) predicted from Eq. (8). This expression accounts for approximately 65% of the intermodel variance in H and tends to accurately predict values of H for GCMs with a variety of AMOC strengths (Fig. 3a). Note that Eq. (8) generally under-predicts the magnitude of H in most GCMs.

Isolating the intermodel spread in F_b, N^2, and $\Delta_y \rho$ by fixing two variables as the multi-model mean and applying the intermodel spread of the other variable, allows us to understand how the intermodel spread in North Atlantic processes relate to the intermodel spread in H. Intermodel variations in F_b and N^2 dominate the intermodel spread in H, accounting for approximately 40% and 60% of the intermodel variance. $\Delta_y \rho$ contributes very little to the intermodel variance in H (Fig. 3b).

4 Discussion and conclusions

Coupled GCMs exhibit a large intermodel spread in the mean-state AMOC, with strengths varying between 12 and 25 Sv (Fig. 1). In this study, we introduce a framework for understanding the intermodel spread in the AMOC strength across GCMs by assessing the thermal-wind expression and surface water mass transformation.

We find that the intermodel spread in the AMOC strength can be approximated by the thermal-wind expression (Eq. 2). These results build on earlier work by De Boer et al. (2010), which showed that the thermal-wind expression accurately approximates the AMOC strength in ocean-only models. Here, we show that the thermal-wind expression accurately approximates the AMOC strength in more comprehensive coupled GCMs. We further show that intermodel variations in H contribute most to intermodel variations in the AMOC strength (Fig. 2). GCMs with a deeper H tend to have a stronger AMOC. We further link H to North Atlantic surface water mass transformation (Eq. 7 and Fig. 3) to relate H to properties of the North Atlantic. We find that GCMs with a deeper H tend to also have stronger surface buoyancy loss and weaker stratification in the North Atlantic.

Together the thermal wind and surface water mass transformation frameworks allow us to summarize the AMOC strength in GCMs as a function of several key ocean features (Figure 4). Specifically, we show that the intermodel spread in the Atlantic basin meridional density difference $\Delta_y \rho$ contributes little to the intermodel spread in AMOC strength across GCMs. Thus, GCMs with strong $\Delta_y \rho$ (Fig. 4a) or weak $\Delta_y \rho$ (Fig. 4b), as indicated by the gradient in color between each density class, exhibit little variation in the mean-state AMOC strength. Instead, the intermodel spread in the AMOC strength across GCMs is related to the intermodel spread in the overturning scale depth H. GCMs with a weak mean-state AMOC generally exhibit a shallower H (Fig. 4c), while GCMs with a strong mean-state

AMOC generally exhibit a deeper H (Fig. 4d). We also show that GCMs with a deeper H exhibit more North Atlantic surface buoyancy loss (indicated by the blue arrows) and weaker North Atlantic stratification (indicated by the grey lines). In fact, intermodel variations in North Atlantic surface buoyancy loss and stratification account for approximately 40% and 60% of the intermodel variance in H, respectively. However, because we examined steady-state simulations, the causality is unclear. Future work should examine whether a deeper H leads to a stronger AMOC and thus more surface buoyancy loss and weaker stratification in the North Atlantic, or if stronger surface buoyancy loss leads to weaker stratification, a deeper H, and a stronger AMOC.

A key implication of this work is that constraining the intermodel spread in H may ultimately constrain the intermodel spread in the AMOC strength across GCMs. Here, we introduced a perspective that details North Atlantic controls on the depth of H, by linking North Atlantic surface buoyancy loss and stratification to H (Eq. 8). Our results imply that reducing the intermodel spread in North Atlantic surface buoyancy loss could reduce the intermodel spread in H and, therefore, the AMOC strength. For example, better representing shortwave and longwave cloud radiative fluxes or surface winds over the North Atlantic might improve modeled North Atlantic surface buoyancy loss and reduce the intermodel spread in H and thus the AMOC strength.

However, other studies show that H depends strongly on interior ocean processes, such as vertical diffusivity (Klinger & Marotzke, 1999; Marotzke & Klinger, 2000; Nikurashin & Vallis, 2012), or on Southern Ocean processes, such as Ekman and eddy transport (Toggweiler & Samuels, 1998; Gnanadesikan, 1999; Nikurashin & Vallis, 2012; Thompson et al., 2016; Marshall et al., 2017), which implies other sources of intermodel spread in H. Additionally, recent work has argued that low-latitude processes can also play an important role in setting the Atlantic basin stratification and thus H (e.g., Newsom & Thompson, 2018; Cessi, 2019; Newsom et al., 2021), which implies that H may also be controlled by inter-basin ocean dynamics. However, it is thus far unclear how to reconcile the nonlocal perspective on H with the local, North Atlantic perspective introduced in this study.

Constraining the intermodel spread in H may also help to constrain the climate response to greenhouse-gas forcing. Several studies have shown a clear link between the depth of the AMOC and the depth of ocean heat storage under warming (Kostov et al., 2014; Saenko et al., 2018; J. M. Gregory et al., 2023). While these studies largely attribute this link to Southern Ocean processes (Kuhlbrodt & Gregory, 2012; Saenko et al., 2018; Newsom et al., 2023), it suggests that constraining H might constrain the the transient climate response. Furthermore, because the mean-state AMOC strength is related to future AMOC changes (J. Gregory et al., 2005; Weaver et al., 2012; Winton et al., 2014; Weijer et al., 2020; Bonan et al., 2022), our work also implies that improving mean-state processes that impact H, whether it be locally in the North Atlantic or non-locally in the Southern Ocean, will ultimately lead to a better understanding of how the AMOC changes under warming.

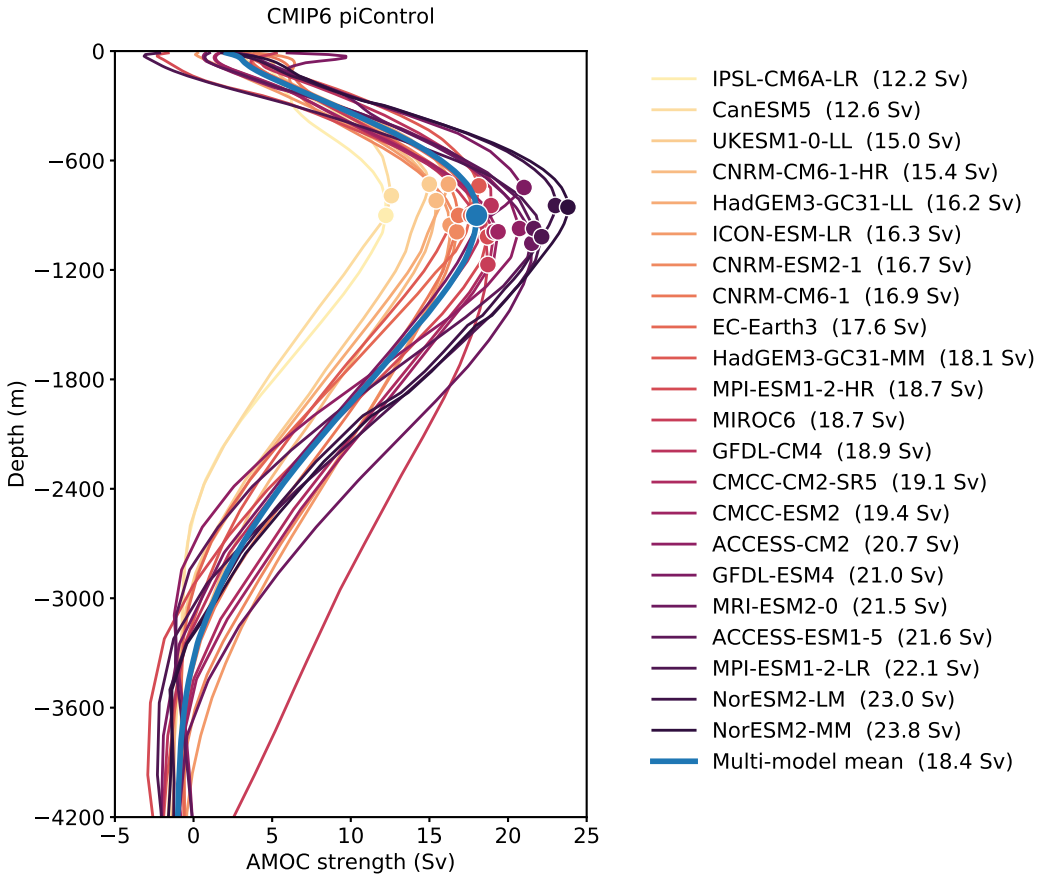

Figure 1. The mean-state AMOC in CMIP6 climate models. Profile of the meridional overturning streamfunction in the Atlantic basin at the latitude of maximum AMOC strength (poleward of 30°N) for each CMIP6 piControl simulation. The circle markers denote the maximum AMOC strength for each GCM. The maximum AMOC strength is also listed next to each climate model name in the legend. Climate models are listed and color coded from weakest-to-strongest mean-state AMOC strength. The blue line is the multi-model mean AMOC.

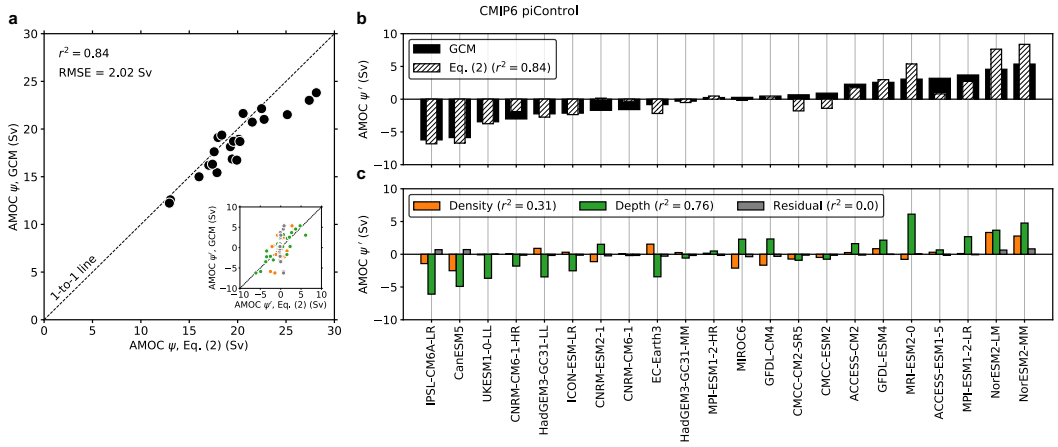

Figure 2. Controls on the AMOC strength. (a) Scatter plot of the AMOC strength predicted by the thermal-wind expression (Eq. 2) versus the AMOC strength diagnosed from the climate models. (b) Bar plot showing the intermodel spread in the AMOC strength predicted by the thermal-wind expression (Eq. 2) and diagnosed from the climate models. (c) Bar plot showing the contribution of the three terms in Eq. (4) to the intermodel spread in the AMOC strength. Climate models are ordered from weakest-to-strongest mean-state AMOC strength for (b) and (c). The proportion of variance explained is in the legend of each sub-panel figure. Panel (a) contains a subset figure that shows how each term in Eq. (4) contributes to the intermodel spread in the AMOC strength.

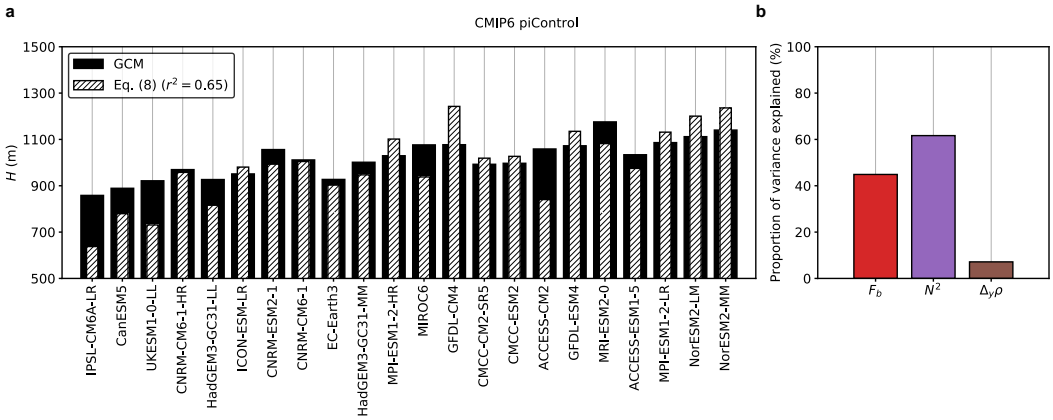

Figure 3. Connection between the overturning scale depth H and the North Atlantic. (a) Bar plot showing (solid black) H diagnosed from the climate models and (hatch black) H predicted by Eq. (8). Climate models are ordered from weakest-to-strongest mean-state AMOC strength. (b) Bar plot showing the proportion of variance explained by the intermodel variance in (red) North Atlantic surface buoyancy loss F_b, (pruple) North Atlantic stratification N^2, and (brown) the meridional density difference in the Atlantic basin $\Delta_y\rho$. Climate models are ordered from weakest-to-strongest mean-state AMOC strength for (a).

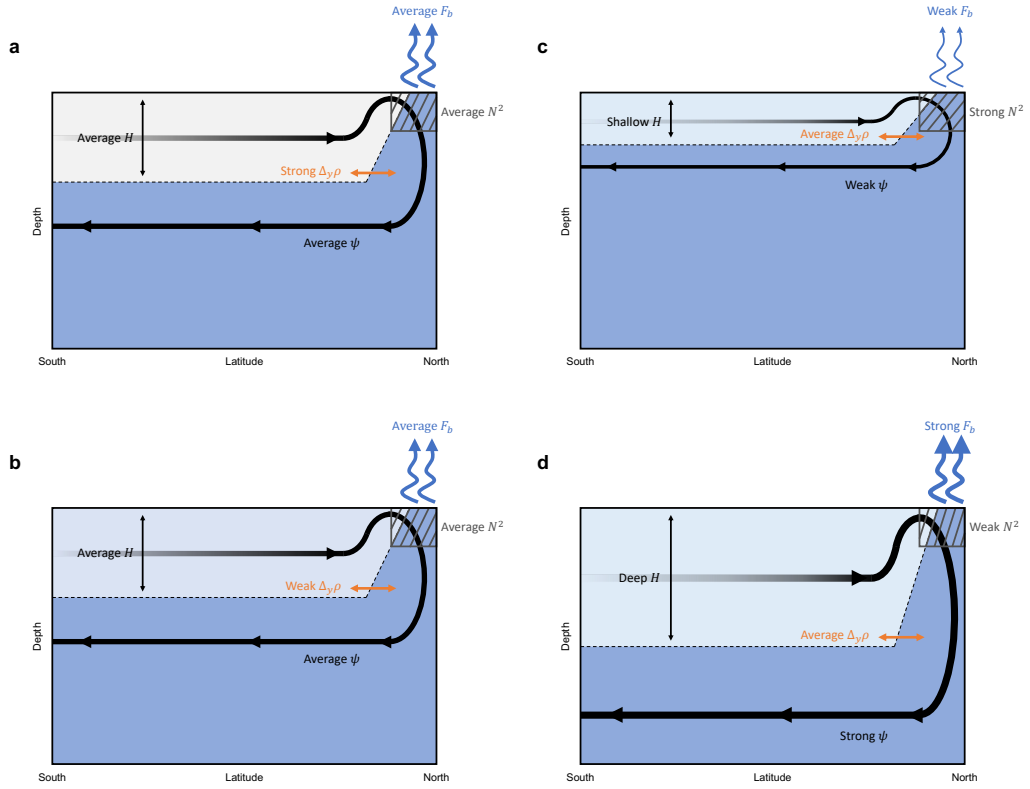

Figure 4. Schematic describing controls on the AMOC in CMIP6. A schematic describing the processes in climate models that are associated with a weak mean-state AMOC and a strong mean-state AMOC. The dashed line denotes the overturning scale depth (H). The streamline denotes the meridonal overturning streamfunction or AMOC strength (ψ). The blue arrows denote surface buoyancy loss in the North Atlantic (F_b). The grey box denotes the magnitude of North Atlantic stratification (N^2). The orange arrow and colors of each density layer denotes the meridional density difference ($\Delta_y\rho$). Climate models with (a) stronger or (b) weaker $\Delta_y\rho$ tend to have similar AMOC strengths. However, climate models with a (c) shallower or (d) deeper H tend to have a weaker or a stronger AMOC strength, weaker or stronger F_b, and stronger or weaker N^2, respectively.

Acknowledgments

M.S.N is grateful for Caltech's Summer Undergraduate Research Fellowship (SURF) program and the Department of Physics at The Ohio State University for support of this research. D.B.B was supported by the National Science Foundation (NSF) Graduate Research Fellowship Program (NSF Grant DGE1745301). E.R.N was supported by NSF Grant OCE-2048576 and M2LInES research funding by the generosity of Eric and Wendy Schmidt by recommendation of the Schmidt Futures program. A.F.T was supported by NSF Grant OCE-2023259.

Open Research

The authors thank the climate modeling groups for producing and making available their model output, which is accessible at the Earth System Grid Federation (ESGF) Portal (https://esgf-node.llnl.gov/search/cmip6/). A list of the CMIP6 models used in this study is provided in Figure 1 and described in Section 2.1.

References

Abernathey, R., Marshall, J., & Ferreira, D. (2011, 12). The dependence of southern ocean meridional overturning on wind stress. *Journal of Physical Oceanography*, *41*, 2261-2278. doi: 10.1175/JPO-D-11-023.1

Baker, J. A., Watson, A. J., & Vallis, G. K. (2020). Meridional overturning circulation in a multibasin model. Part I: dependence on Southern Ocean buoyancy forcing. *Journal of Physical Oceanography*, *50*(5), 1159–1178.

Bonan, D. B., Thompson, A. F., Newsom, E. R., Sun, S., & Rugenstein, M. (2022). Transient and equilibrium responses of the Atlantic overturning circulation to warming in coupled climate models: the role of temperature and salinity. *Journal of Climate*, *35*(15), 5173–5193.

Broecker, W. S. (1991). The great ocean conveyor. *Oceanography*, *4*(2), 79–89.

Buckley, M. W., & Marshall, J. (2016). Observations, inferences, and mechanisms of the Atlantic Meridional Overturning Circulation: A review. *Reviews of Geophysics*, *54*(1), 5-63.

Cessi, P. (2019). The Global Overturning Circulation. *Annual Review of Marine Science*, *11*(1), 249-270.

Cheng, W., Chiang, J. C. H., & Zhang, D. (2013). Atlantic meridional overturning circulation (amoc) in cmip5 models: Rcp and historical simulations. *Journal of Climate*, *26*(18), 7187 - 7197.

De Boer, A. M., Gnanadesikan, A., Edwards, N. R., & Watson, A. J. (2010). Meridional density gradients do not control the Atlantic overturning circulation. *Journal of Physical Oceanography*, *40*(2), 368–380.

Ferrari, R., Jansen, M. F., Adkins, J. F., Burke, A., Stewart, A. L., & Thompson, A. F. (2014). Antarctic sea ice control on ocean circulation in present and glacial climates. *Proceedings of the National Academy of Sciences*, *111*(24), 8753–8758.

Frierson, D. M., Hwang, Y.-T., Fučkar, N. S., Seager, R., Kang, S. M., Donohoe, A., ... Battisti, D. S. (2013). Contribution of ocean overturning circulation to tropical rainfall peak in the Northern Hemisphere. *Nature Geoscience*, *6*(11), 940–944.

Ganachaud, A., & Wunsch, C. (2003). Large-scale ocean heat and freshwater transports during the world ocean circulation experiment. *Journal of Climate*, *16*(4), 696 - 705.

Gent, P. R. (2016). Effects of southern hemisphere wind changes on the meridional overturning circulation in ocean models. *Annual review of marine science*, *8*, 79–94.

Gnanadesikan, A. (1999, 04). A Simple Predictive Model for the Structure of the Oceanic Pycnocline. *Science (New York, N.Y.)*, *283*, 2077-9. doi: 10.1126/science.283.5410.2077

Gordon, A. L. (1986). Interocean exchange of thermocline water. *Journal of Geophysical Research: Oceans*, *91*(C4), 5037–5046.

Gregory, J., Dixon, K., Stouffer, R., Weaver, A., Driesschaert, E., Eby, M., ... others (2005). A model intercomparison of changes in the Atlantic thermohaline circulation in response to increasing atmospheric CO2 concentration. *Geophysical Research Letters*, *32*(12).

Gregory, J. M., Bloch-Johnson, J., Couldrey, M. P., Exarchou, E., Griffies, S. M., Kuhlbrodt, T., ... Zanna, L. (2023). *A new conceptual model of global ocean heat uptake* (No. 0123456789). Springer Berlin Heidelberg. Retrieved from `https://doi.org/10.1007/s00382-023-06989-z` doi: 10.1007/s00382-023-06989-z

Heuzé, C. (2021). Antarctic bottom water and North Atlantic deep water in CMIP6 models. *Ocean Science*, *17*(1), 59–90.

Hughes, T. M. C., & Weaver, A. J. (1994). Multiple equilibria of an asymmetric two-basin ocean model. *Journal of Physical Oceanography*, *24*(3), 619 - 637.

Jackson, L., & Petit, T. (2023). North Atlantic overturning and water mass transformation in CMIP6 models. *Climate Dynamics*, *60*(9-10), 2871–2891.

Jansen, M. F., & Nadeau, L.-P. (2016). The effect of Southern Ocean surface buoyancy loss on the deep-ocean circulation and stratification. *Journal of Physical Oceanography*, *46*(11), 3455–3470.

Jansen, M. F., Nadeau, L.-P., & Merlis, T. M. (2018). Transient versus equilibrium response of the ocean's overturning circulation to warming. *Journal of Climate*, *31*(13), 5147–5163.

Jochum, M., & Eden, C. (2015). The connection between Southern Ocean winds, the Atlantic meridional overturning circulation, and Indo-Pacific upwelling. *Journal of Climate*, *28*(23), 9250–9257.

Johnson, H. L., Cessi, P., Marshall, D. P., Schloesser, F., & Spall, M. A. (2019). Recent contributions of theory to our understanding of the atlantic meridional overturning circulation. *Journal of Geophysical Research: Oceans*, *124*(8), 5376-5399.

Klinger, B. A., & Marotzke, J. (1999). Behavior of double-hemisphere thermohaline flows in a single basin. *Journal of physical oceanography*, *29*(3), 382–399.

Kostov, Y., Armour, K. C., & Marshall, J. (2014). Impact of the Atlantic Meridional Overturning Circulation on Ocean Heat Storage and Transient Climate Change. *Geophysical Research Letters*.

Kuhlbrodt, T., & Gregory, J. M. (2012). Ocean heat uptake and its consequences for the magnitude of sea level rise and climate change. *Geophysical Research Letters*, *39*(17), 1–6. doi: 10.1029/2012GL052952

Lin, Y.-J., Rose, B. E., & Hwang, Y.-T. (2023). Mean state AMOC affects AMOC weakening through subsurface warming in the Labrador Sea. *Journal of Climate*, *36*(12), 3895–3915.

Lumpkin, R., & Speer, K. (2007). Global ocean meridional overturning. *Journal of Physical Oceanography*, *37*(10), 2550–2562.

Mahajan, S., Zhang, R., & Delworth, T. L. (2011). Impact of the Atlantic meridional overturning circulation (AMOC) on Arctic surface air temperature and sea ice variability. *Journal of Climate*, *24*(24), 6573–6581.

Marotzke, J., & Klinger, B. A. (2000). The dynamics of equatorially asymmetric thermohaline circulations. *Journal of physical oceanography*, *30*(5), 955–970.

Marshall, J., Donohoe, A., Ferreira, D., & McGee, D. (2014). The ocean's role in setting the mean position of the Inter-Tropical Convergence Zone. *Climate Dynamics*, *42*, 1967–1979.

Marshall, J., & Radko, T. (2003). Residual-mean solutions for the Antarctic Circumpolar Current and its associated overturning circulation. *Journal of Physical Oceanography*, *33*(11), 2341–2354.

Marshall, J., Scott, J. R., Romanou, A., Kelley, M., & Leboissetier, A. (2017). The dependence of the ocean's MOC on mesoscale eddy diffusivities: A model study. *Ocean Modelling*, *111*, 1–8. Retrieved from `http://dx.doi.org/10.1016/j.ocemod.2017.01.001` doi: 10.1016/j.ocemod.2017.01.001

Newsom, E. R., & Thompson, A. F. (2018). Reassessing the role of the Indo-Pacific in the ocean's global overturning circulation. *Geophysical Research Letters*, *45*(22), 12–422.

Newsom, E. R., Thompson, A. F., Adkins, J. F., & Galbraith, E. D. (2021). A hemispheric asymmetry in poleward ocean heat transport across climates: Implications for overturning and polar warming. *Earth and Planetary Science Letters*, *568*, 117033.

Newsom, E. R., Zanna, L., & Gregory, J. M. (2023). Background Pycnocline Depth Constrains Future Ocean Heat Uptake Efficiency. *Geophysical Research Letters*, *50*(22), 1–11. doi: 10.1029/2023GL105673

Nikurashin, M., & Vallis, G. (2012). A theory of the interhemispheric meridional overturning circulation and associated stratification. *Journal of Physical Oceanography*, *42*(10), 1652–1667.

Radko, T., & Kamenkovich, I. (2011). Semi-adiabatic model of the deep stratification and meridional overturning. *Journal of physical oceanography*, *41*(4), 757–780.

Reintges, A., Martin, T., Latif, M., & Keenlyside, N. S. (2017). Uncertainty in twenty-first century projections of the Atlantic Meridional Overturning Circulation in CMIP3 and CMIP5 models. *Climate Dynamics*, *49*, 1495–1511.

Saenko, O. A., Yang, D., & Gregory, J. M. (2018). Impact of mesoscale eddy transfer on heat uptake in an eddy-parameterizing ocean model. *Journal of Climate*, *31*(20), 8589–8606. doi: 10.1175/JCLI-D-18-0186.1

Samelson, R. (2009). A simple dynamical model of the warm-water branch of the middepth meridional overturning cell. *Journal of physical oceanography*, *39*(5), 1216–1230.

Schmittner, A., Latif, M., & Schneider, B. (2005). Model projections of the North Atlantic thermohaline circulation for the 21st century assessed by observations. *Geophysical research letters*, *32*(23).

Sévellec, F., & Fedorov, A. V. (2011). Stability of the Atlantic meridional overturning circulation and stratification in a zonally averaged ocean model: Effects of freshwater flux, Southern Ocean winds, and diapycnal diffusion. *Deep Sea Research Part II: Topical Studies in Oceanography*, *58*(17-18), 1927–1943.

Sévellec, F., & Fedorov, A. V. (2016). AMOC sensitivity to surface buoyancy fluxes: Stronger ocean meridional heat transport with a weaker volume transport? *Climate Dynamics*, *47*(5-6), 1497–1513.

Shakespeare, C. J., & Hogg, A. M. (2012). An analytical model of the response of the meridional overturning circulation to changes in wind and buoyancy forcing. *Journal of Physical Oceanography*, *42*(8), 1270 - 1287. Retrieved from `https://journals.ametsoc.org/view/journals/phoc/42/8/jpo-d-11-0198.1.xml` doi: https://doi.org/10.1175/JPO-D-11-0198.1

Sigmond, M., Fyfe, J. C., Saenko, O. A., & Swart, N. C. (2020). Ongoing AMOC and related sea-level and temperature changes after achieving the Paris targets. *Nature Climate Change*, *10*(7), 672–677.

Speer, K., & Tziperman, E. (1992). Rates of water mass formation in the North Atlantic Ocean. *Journal of Physical Oceanography*, *22*(1), 93–104.

Stommel, H. (1961). Thermohaline convection with two stable regimes of flow. *Tellus*, *13*(2), 224-230.

Talley, L. D. (2013). Closure of the global overturning circulation through the Indian, Pacific, and Southern Oceans: Schematics and transports. *Oceanography*, *26*(1), 80–97.

Thompson, A. F., Stewart, A. L., & Bischoff, T. (2016). A multibasin residual-mean model for the global overturning circulation. *Journal of Physical Oceanography*, *46*(9).

Thorpe, R. B., Gregory, J. M., Johns, T. C., Wood, R. A., & Mitchell, J. F. B. (2001). Mechanisms determining the atlantic thermohaline circulation response to greenhouse gas forcing in a non-flux-adjusted coupled climate model. *Journal of Climate*, *14*(14), 3102 - 3116.

Toggweiler, J., & Samuels, B. (1998). On the ocean's large-scale circulation near the limit of no vertical mixing. *Journal of Physical Oceanography*, *28*(9), 1832–1852.

Vallis, G. K. (2000). Large-scale circulation and production of stratification: Effects of wind, geometry, and diffusion. *Journal of Physical Oceanography*, *30*(5), 933–954.

Wang, C., Dong, S., & Munoz, E. (2010). Seawater density variations in the North Atlantic and the Atlantic meridional overturning circulation. *Climate dynamics*, *34*, 953–968.

Weaver, A. J., Sedláček, J., Eby, M., Alexander, K., Crespin, E., Fichefet, T., ... others (2012). Stability of the Atlantic meridional overturning circulation: A model intercomparison. *Geophysical Research Letters*, *39*(20).

Weijer, W., Cheng, W., Garuba, O. A., Hu, A., & Nadiga, B. T. (2020). CMIP6 Models Predict Significant 21st Century Decline of the Atlantic Meridional Overturning Circulation. *Geophysical Research Letters*, *47*(12), e2019GL086075.

Winton, M., Anderson, W. G., Delworth, T. L., Griffies, S. M., Hurlin, W. J., & Rosati, A. (2014). Has coarse ocean resolution biased simulations of transient climate sensitivity? *Geophysical Research Letters*, *41*(23), 8522–8529.

Wolfe, C. L., & Cessi, P. (2010). What sets the strength of the middepth stratification and overturning circulation in eddying ocean models? *Journal of Physical Oceanography*, *40*(7), 1520–1538.

Wolfe, C. L., & Cessi, P. (2011). The adiabatic pole-to-pole overturning circulation. *Journal of Physical Oceanography*, *41*(9), 1795–1810.

Youngs, M. K., Ferrari, R., & Flierl, G. R. (2020). Basin-width dependence of northern deep convection. *Geophysical Research Letters*, *47*(15), e2020GL089135.

Zhang, R., & Delworth, T. L. (2006). Impact of Atlantic multidecadal oscillations on India/Sahel rainfall and Atlantic hurricanes. *Geophysical research letters*, *33*(17).

Zhang, R., Sutton, R., Danabasoglu, G., Kwon, Y.-O., Marsh, R., Yeager, S. G., ... Little, C. M. (2019). A review of the role of the Atlantic meridional overturning circulation in Atlantic multidecadal variability and associated climate impacts. *Reviews of Geophysics*, *57*(2), 316–375.